Linear geophysical inversion with seismic image-guided kriging

Jack B. Muir*

Fleet Space Technologies, Adelaide, Australia
Research School of Earth Sciences, Australian National University, Canberra, Australia

September 7, 2026

Abstract

Linear geophysical inversions, such as the mapping of surface gravity anomaly to subsurface density anomaly, are a cornerstone of geophysical practice. However, the high degree of ill-posedness of such problems makes interpretation of the resulting subsurface models challenging. I develop a methodology to combine surface potential field measurements, direct subsurface sampling through scout boreholes, and seismic reflection imaging, to generate consistent subsurface anomaly models of significantly greater accuracy and interpretability.

The method relies on non-stationary, anisotropic Gaussian process priors, with the anisotropy derived from image processing of seismic reflection data. Cast into the language of geostatistics, the method could be referred to as seismic image-guided kriging. We validate the method on a synthetic example cropped from the Marmousi2 seismic benchmark, and find that the use of the image-guided prior resulted in a 39% improvement in correlation with the unknown true density anomaly compared to use of a stationary prior.

Key words: Geostatistical simulation, inversion, seismic imaging

1 Introduction

Subsurface inferences based on linear inverse problems play a key role in exploration decision making. Gravity and magnetic data, in particular, remain foundational exploration tools and are commonly inverted to provide 3D images of subsurface density and magnetic susceptibility anomalies, which are then interpreted to reflect bulk-scale petrophysical links to mineralogy.

It is reasonably well known, however, that potential field data is particularly ill-posed (Oldenburg and Pratt, 2007, e.g), and that therefore interpretation of such data is highly non-unique. Much effort has been given to opinionated regularization methods that impose greater geological structure on potential field inversions, thereby increasing interpretability of the anomalies recovered. One must always remember, however, that there is significant residual non-uniqueness in the solution for any reasonable regularization scheme, and that consequently a probabilistic solution that can simulate realistic point-wise (nugget effect) and spatial-correlation variability within its posterior will allow the fairest basis on which interpretations may be made. In the probabilistic framework, regularization imposed through the overall objective function can be interpreted as prior probability functions. In addition, decoupling the effect of parameterization from the effect of regularization/prior is generally desirable in a "continuous" setting (i.e. where the parameterization itself is not designed to induce regularization as would be the case in geological object inversion).

Valentine and Sambridge (2020) give a general theory for continuous linear geophysical inverse problems with a wide range of priors induced by Gaussian processes (GPs, e.g. kriging-style priors). However, in their work they focus on development of theory, and consequently do not fully explore the

*jack.muir@fleet.space

flexible possibilities of GP priors for inversion. In this paper, we investigate non-stationary, anisotropic GP priors induced from image processing of seismic reflection data. By making use of the structural information provided by these images, we can arrive at a fully probabilistic and geologically consistent subsurface model, which can directly combine both surface potential field and downhole petrophysical measurements.

2 Tying seismic images to linear geophysical inversion through Gaussian Markov random fields

The underlying method of the proposed inversion scheme relies on the stochastic partial differential equation (SPDE) approach to approximating Gaussian processes formalized by Lindgren et al. (2011). In particular, we make use of the non-stationary Matérn covariance model proposed by Hale (2014), which shows that the action of a linear operator approximating the desired covariance can be obtained by solving the partial differential equation

$$|\boldsymbol{D}|^{-\frac{1}{4}}(\boldsymbol{x})(1-\alpha\boldsymbol{\nabla}\cdot\boldsymbol{D}(\boldsymbol{x})\cdot\boldsymbol{\nabla})^{l}(1-\beta\boldsymbol{\nabla}\cdot\boldsymbol{D}(\boldsymbol{x})\cdot\boldsymbol{\nabla})|\boldsymbol{D}|^{-\frac{1}{4}}(\boldsymbol{x})q(\boldsymbol{x})=\gamma p(\boldsymbol{x}). \tag{1}$$

The constants l, α, β depend on the desired shape parameter ν of the underlying Matérn process, and are tabulated in Hale (2014). For a spatial white noise $p(\boldsymbol{x})$, the solutions $q(\boldsymbol{x})$ will have an approximately Matérn distributed covariance with spatially varying local anisotropy defined by the tensor $\boldsymbol{D}(\boldsymbol{x})$, where the local distance metric near a point $\boldsymbol{x}$ is $d(\boldsymbol{x},\boldsymbol{y})=\sqrt{(\boldsymbol{x}-\boldsymbol{y})^T\boldsymbol{D}(\boldsymbol{x})(\boldsymbol{x}-\boldsymbol{y})}$. Intuitively, we may obtain a $\boldsymbol{D}(\boldsymbol{x})$ which promotes continuity along favorable geological structures (such as bedding) and suppresses continuity at unfavorable structures (such as faults). As a synthetic example, we will illustrate this concept through a cropped section of the Marmousi2 elastic model (Martin et al., 2006), from which we take the density model as our target, the wave-equation prestack depth migration (WE-PreSDM) image as our guide, and compute z component surface gravity data from the density anomaly using the Choclo Python code (Soler et al., 2023). The model setup is shown in Figure 1.

2.1 Obtaining the seismic image anisotropy tensor

For this study, we follow Fehmers and Höcker (2003) “Van Gogh” filter for the anisotropy tensor $\boldsymbol{D}(\boldsymbol{x})$, which was further utilized for seismic interpolation by Hale (2009) and Hale (2010):

$$\boldsymbol{D}(\boldsymbol{x})=\sum_{i=1}^{2}\mu_i\boldsymbol{v}_i\boldsymbol{v}_i^T, \tag{2}$$

where $\boldsymbol{v}_i$ are the eigenvectors of the smoothed structure tensor $\boldsymbol{S}_\sigma=\boldsymbol{K}_\sigma\circ(\nabla u)(\nabla u)^T$, u being the reflection image amplitude and $\boldsymbol{K}_\sigma$ a smoothing Gaussian filter with lengthscale σ. The coefficients μ_i can be set to promote desired behavior; in particular we make use of Fehmers and Höcker (2003) continuity factor ϵ to suppress continuity across fault structures and reduce the degree of anisotropy when a reliable gradient cannot be measured due to the migrated image amplitude being close to the noise floor. Figure 2 shows the extraction of anisotropy features used in computing $\boldsymbol{D}(\boldsymbol{x})$ from the WE-PreSDM image. Note that we could use arbitrary symmetric positive-definite $\boldsymbol{D}(\boldsymbol{x})$ for the purposes of this study; extraction of an effective $\boldsymbol{D}(\boldsymbol{x})$ from sparse or mixed data constitutes a future area of research.

2.2 Link to geophysical response

Following Valentine and Sambridge (2020), we assume the i^th piece of data is related to the field $q(\boldsymbol{x})$ by

$$d_i=\int_X w_i(\boldsymbol{x})q(\boldsymbol{x})d\boldsymbol{x} \tag{3}$$

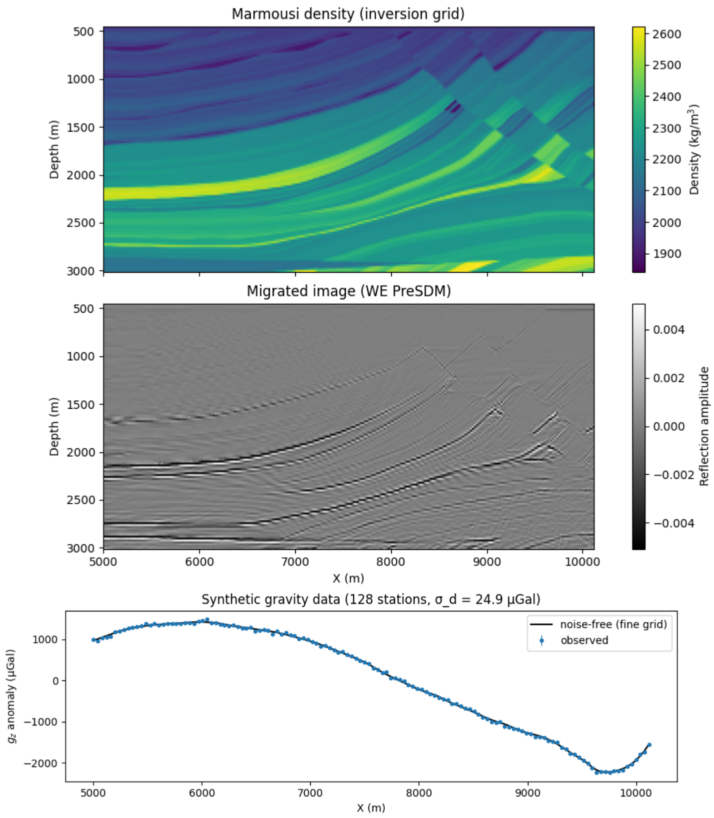

Figure 1. Synthetic data used in this study: Density (upper) and wave-equation prestack depth migration (WE-PreSDM) stack (middle) cropped from the Marmousi2 model; calculated gravity anomaly (bottom).

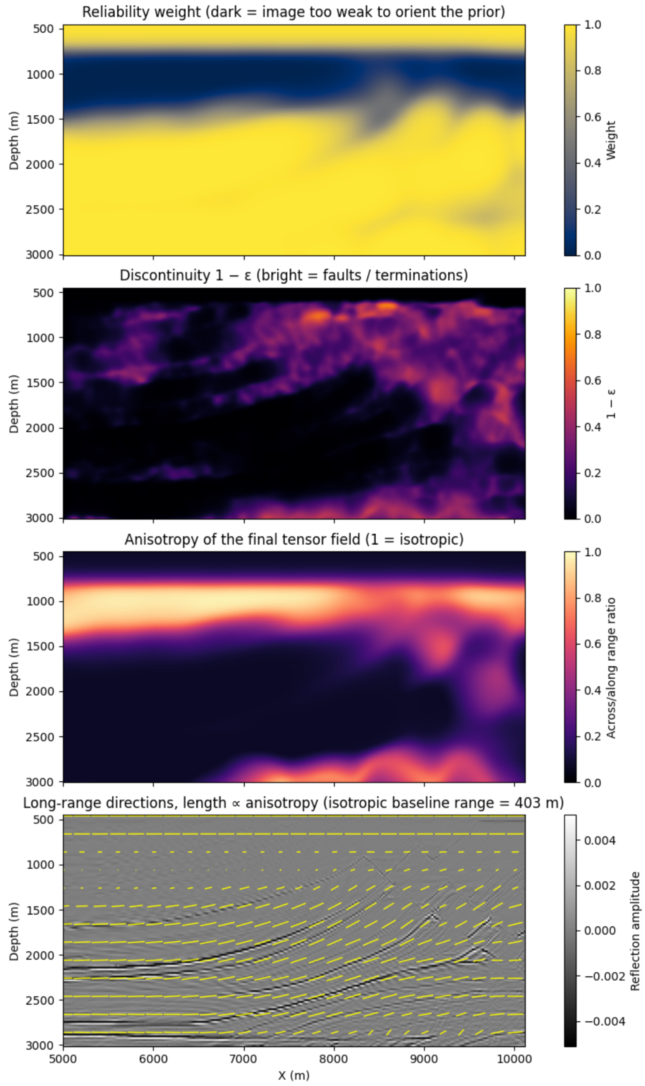

Figure 2. Anisotropy reliability (top), discontinuity (middle upper), and anisotropy strength (middle lower) maps derived from the seismic image (bottom). The seismic image shows overlain major axis of anisotropy direction and length scale across the image in yellow lines.

for data representers $w_i(\boldsymbol{x})$. In this case, we consider representers for direct observation, and 2.5D gravity from rectangular prisms (e.g. the gravity Jacobian from Soler et al. (2023)). We let G be the linear action (which may be represented by a matrix) defined by

$$G_i(\cdot) = \int_X w_i(\boldsymbol{x})(\cdot)d\boldsymbol{x}. \tag{4}$$

Defining $H = C_M G^T$, $A = GH + C_d$ for the linear covariance operator C_M approximated by the solution of Equation 1 and observation covariance C_d. Then for prior mean $q_0(\boldsymbol{x})$, we have the posterior mean $\hat{q}(\boldsymbol{x})$ given by

$$\hat{q} = q_0 + HA^{-1}(d - Gq_0). \tag{5}$$

As the action of operator C_M is applied in a matrix-free manner, I employ a randomize-then-optimize approach to efficiently obtain samples from the posterior distribution (Bardsley et al., 2014).

2.3 Results

We compare 6 model evaluations — combinations of isotropic / image-guided prior, and gravity anomaly / borehole sampling / gravity + boreholes. Table 1 show that image-guided, gravity + borehole combination significantly outperforms the other 5 experiments. In particular, the image-guided prior is held constant between image-guided experiments, showing the significant uplift available when both direct borehole measurements (for constraining individual geological features) and geophysical measurements (for constraining bulk properties) are available. Figure 3 shows the mean and standard deviation of the posterior density anomalies recovered for the gravity+borehole case for both the isotropic and image-guided prior cases. Sparse borehole information is not sufficient to characterize the correlation structure in the isotropic case, resulting in a mean density anomaly that is dominated by surface gravity measurements and hence smooth. In the image-guided case, the correlation structure is supplied by the underlying seismic image, allowing borehole information to be propagated consistently with surface gravity measurements. Figure 4 shows simulated draws from the posterior distribution of density anomaly in both the isotropic and image-guided cases, showing the correlation structure induced by the strong amplitudes of the seismic reflector through the center of the images. The upper portion of the image-guided draws show the effect of anisotropy reliability gating in the design of the μ_i coefficients, with the draws returning to isotropic in those areas where the image amplitude is too weak to confidently determine anisotropy.

Data	Prior	Mean RMS Error (kg/m^3)	Corr with Truth	Mean Posterior σ (kg/m^3)
Gravity Only	Stationary	78.3	0.346	82.8
Gravity Only	image-guided	76.7	0.392	88.8
Boreholes Only	Stationary	78.3	0.363	87.3
Boreholes Only	image-guided	70.1	0.548	79.5
Gravity + Boreholes	Stationary	73.4	0.474	75.8
Gravity + Boreholes	image-guided	**63.0**	**0.657**	**72.7**

Table 1. Summary of inversion results for different data and prior combinations. RMS error and correlation are calculated with respect to the true model. Posterior σ is the mean of the posterior standard deviation across the model domain.

3 Conclusions

I have shown how it is possible to guide linear geophysical inverse problems (in this case, a mixture of direct sampling and surface gravity measurements) using anisotropic GP priors derived from seismic

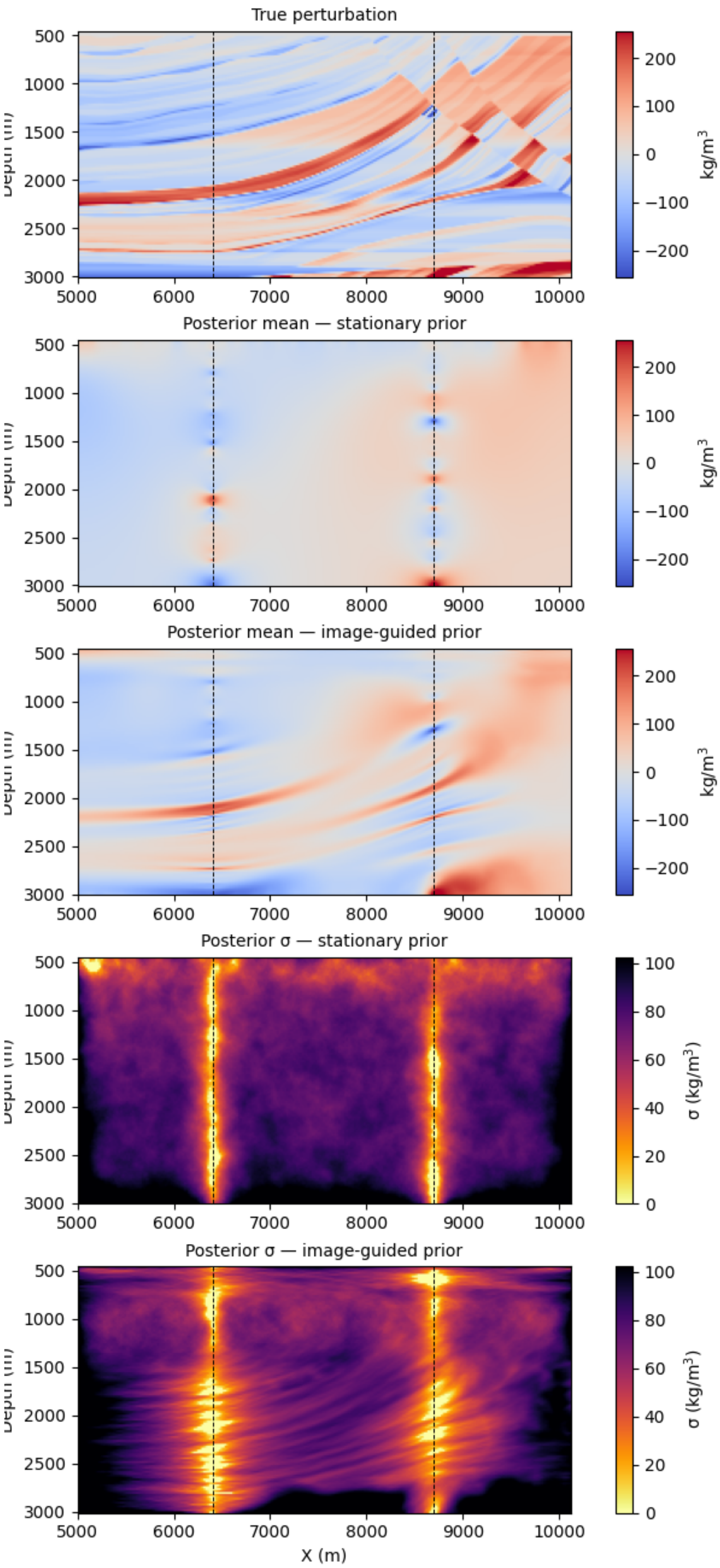

Figure 3. Joint inversion results for the gravity and boreholes data, across stationary and image-guided priors.

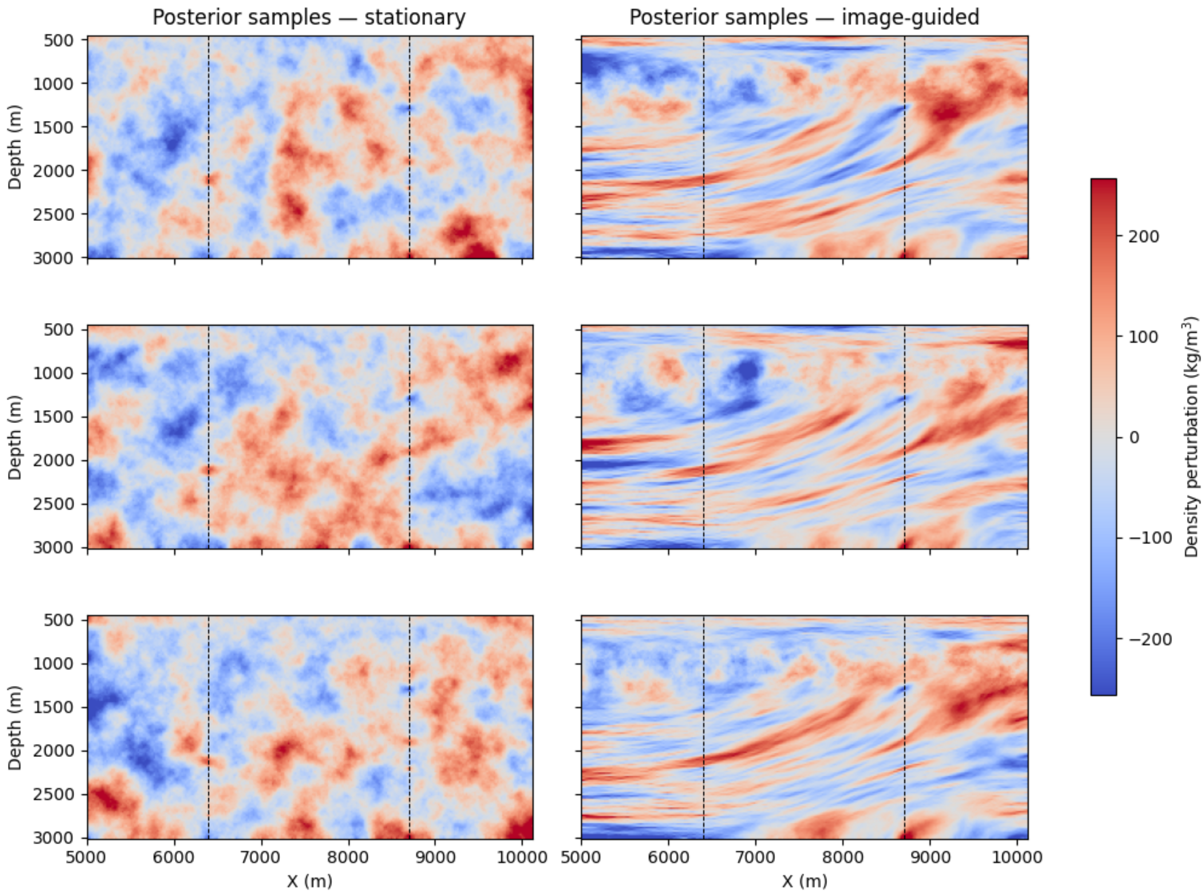

Figure 4. Samples from the posterior distribution for the gravity + boreholes case. Left: stationary prior, Right: image-guided prior.

imagery. This result extends the pure-interpolation result of Hale (2014), which I term seismic image-guided kriging, to the case of general continuous linear inverse problems following the development of Valentine and Sambridge (2020). I show that the addition of geophysical sensing can significantly improve the accuracy and width of the resulting posterior distribution, with corresponding benefits to further inferences drawn from posterior simulation.

Acknowledgments

The author would like to thank Andrej Bona and Esteban Jimenez for productive discussions during the ideation of this study.

References

Bardsley, J. M., Solonen, A., Haario, H., and Laine, M., 2014, Randomize-then-optimize: A method for sampling from posterior distributions in nonlinear inverse problems: SIAM Journal on Scientific Computing, **36**, no. 4, A1895–A1910.

Fehmers, G. C., and Höcker, C. F. W., 2003, Fast structural interpretation with structure-oriented filtering: Geophysics, **68**, no. 4, 1286–1293.

Hale, D., 2009, Image-guided blended neighbor interpolation of scattered data: SEG Technical Program Expanded Abstracts 2009, SEG Technical Program Expanded Abstracts 2009, 1127–1131.

Hale, D., 2010, Image-guided 3D interpolation of borehole data: SEG Technical Program Expanded Abstracts 2010, SEG Technical Program Expanded Abstracts 2010, 1266–1270.

Hale, D., Implementing an anisotropic and spatially varying Matérn model covariance with smoothing filters:, Technical Report CWP-815, Center for Wave Phenomena, Colorado School of Mines, 2014.

Lindgren, F., Rue, H., and Lindström, J., 2011, An explicit link between Gaussian fields and Gaussian Markov random fields: The stochastic partial differential equation approach: Journal of the Royal Statistical Society Series B: Statistical Methodology, **73**, no. 4, 423–498.

Martin, G. S., Wiley, R., and Marfurt, K. J., 2006, Marmousi2: An elastic upgrade for Marmousi: The Leading Edge, **25**, no. 2, 156–166.

Oldenburg, D., and Pratt, D., 2007, Geophysical inversion for mineral exploration: A decade of progress in theory and practice: Proceedings of Exploration 07: Fifth Decennial International Conference on Mineral Exploration, 61–95.

Soler, S. R., Uieda, L., and Fatiando a Terra Project. Choclo: Kernel functions for forward modelling of gravity and magnetic fields in Python:. `https://github.com/fatiando/choclo`, 2023. Software; no registered DOI located at time of writing.

Valentine, A. P., and Sambridge, M., 2020, Gaussian process models—I. a framework for probabilistic continuous inverse theory: Geophysical Journal International, **220**, no. 3, 1632–1647.